Disponible en www.hormigonyacero.com
Hormigón y Acero, 2023
https://doi.org/10.33586/hya.2023.3131

ARTÍCULO EN AVANCE ON LINE

Blast Absorption Capacity of Brittle Mineral Foam: an Experimental Evaluation

Aldjabar Aminou, Mohamed Ben-Rhouma, Bachir Belkassem, Hamza Ousji, Oussama Atoui, Lincy Pyl, David Lecompte

DOI: https://doi.org/10.33586/hya.2023.3131

Para ser publicado en: *Hormigón y Acero*
Por favor, el presente artículo debe ser citado así:
Aminou, A., Ben-Rhouma, M., Belkassem, B., Ousji, H., Atoui, O., Pyl, L., & Lecompte,D. (2023) **Blast Absorption Capacity of Brittle Mineral Foam: an Experimental Evaluation**, *Hormigón y Acero*, doi: https://doi.org/10.33586/hya.2023.3131

Blast absorption capacity of brittle mineral foam: an experimental evaluation

Aldjabar Aminou*, PhD student

Royal Military Academy, Civil and Materials Engineering Department, 30 Avenue de la Renaissance, 1000 Brussels, Belgium, aldjabaraminou@hotmail.com

Mohamed Ben Rhouma, PhD student

Royal Military Academy, Civil and Materials Engineering Department, 30 Avenue de la Renaissance, 1000 Brussels, Belgium, mohamed.benrouhma@mil.be

Bachir Belkassem, Researcher

Royal Military Academy, Civil and Materials Engineering Department, 30 Avenue de la Renaissance, 1000 Brussels, Belgium, bachir.belkassem@hotmail.com

Hamza Ousji, Assistant Professor

Military Research Center, Sciences and Technologies for Defense, Cité Taieb Mhiri, Aouina, 2045 Tunis, Tunisia, hamzaousji@gmail.com

Oussama Atoui, PhD Student

Vrije Universiteit Brussel (VUB), Mechanics of Materials and Construction Department, Pleinlaan 2, 1050 Brussels, Belgium

Royal Military Academy, Civil and Materials Engineering Department, 30 Avenue de la Renaissance, 1000 Brussels, Belgium, oussama.atoui@vub.be

Lincy Pyl, Professor

Vrije Universiteit Brussel (VUB), Mechanics of Materials and Constructions Department, Pleinlaan 2, 1050 Brussels, Belgium, lincy.pyl@vub.be

David Lecompte, Professor

Royal Military Academy, Civil and Materials Engineering Department, 30 Avenue de la Renaissance, 1000 Brussels, Belgium, david.lecompte@mil.be

*Corresponding author.

Email address: aldjabaraminou@hotmail.com

Abstract Cellular materials, such as aluminum foam, have proven to be effective energy absorbents. They can be used as the crushable core for blast mitigation sacrificial cladding. In this paper insights into the blast response of a brittle mineral foam-based sacrificial cladding are presented. The experimental set-up used consists of a rigid steel frame (1000 mm × 1000 mm × 15 mm) with a square cavity of 300 mm x 300 mm in the center. An aluminum plate, representing the structure, with a total surface of 400 mm × 400 mm and a thickness of 2 mm is clamped into the steel frame. Two synchronized high-speed cameras in a stereoscopic configuration are used to capture the dynamic response of the aluminum plate at a frame rate of 20000 frames per second. The transient deformation fields are computed using a three-dimensional digital image correlation technique. The blast load is obtained by detonating 20 g of C4 placed at a distance of 250 mm from the center of the tested aluminum plate. The absorption capacity of the brittle mineral foam is assessed by comparing the out-of-plane displacement, the velocity, the acceleration and the major principal strain of the thin aluminum plate with and without the protective mineral foam. Two foam configurations with different thicknesses are considered: 60 mm and 120 mm. It is shown that adding the brittle mineral foam reduces the out-of-plane displacement together with the displacement velocity and acceleration of the aluminum plate at least by a factor of two. Post-mortem analysis of the foams shows that mitigation of the blast load in the present set-up and under the considered loading is partially obtained by crushing of the cell walls but mostly though the growth of cracks in the specimen.

Keywords Blast mitigation – Sacrificial cladding – Brittle mineral foam – Vehicle protection

1. Introduction

The demand for blast-resistant structures is growing as a result of the high number of casualties caused by improvised explosive devices (IEDs) and landmine attacks [1]. On the battlefield about 50 to 60 % of all cases of injury and fatality are caused by IEDs [2]. Due to potential significant deformation of a vehicle's bottom plate and high accelerations inside the vehicle, explosion attacks can easily cause significant harm to occupants [3]. The general concept of blast protection is to insert a structure between the explosive charge and the target [4]. This structure is designed to either mitigate explosive detonation [5]–[7], disrupt blast wave propagation [4], [8]–[10], or provide passive target protection [11]–[13]. The detonation of the explosive can for example be mitigated by using bulk water [5], mist [6] and aqueous foam [7]. Multi-layered materials on the other hand rely on the impedance mismatch between each layer to disperse the blast waves across the structure [8]. The incoming blast wave can be deflected or disturbed by using specific geometries, such as V-shaped plates [9], arrays of cylindrical pipes [10] or 3D grid plates [4]. The sacrificial cladding is a passive protective solution that allows the blast wave

energy to be dissipated and enhances the protection of the target against blast load [14]. Sacrificial claddings consist of a crushable material positioned in between the structure to be protected and a front skin [14], [15]. The purpose of this front skin is to distribute the generated blast pressure onto the crushable core and to ensure its uniform compression [12], [14], [16]. The crushable core gradually deforms under constant low stress compared to the resistance of the target, absorbing most of the blast-induced energy and therefore potentially safeguarding the target [17].

The crushable core commonly consists of a cellular material with several possible topologies, including tubular [18]–[20], honeycomb structures [17], [21], auxetic cores [21], [22] or cellular solids such as metallic [15], [23], [24], polymeric [14], [25]–[27], or mineral foam [28], [29]. Bonsmann et al. [19], [20] used metallic thin-walled cylinders with and without polyurea coating as crushable cores to mitigate vertical acceleration experienced by passengers in a vehicle subjected to blast loading. It was shown that by using a thin-walled cylinder alone, vertical acceleration levels can be reduced from 150 g to roughly 10 g. At very high acceleration levels, the addition of a polyurea coating to the thin-walled cylinders can result in an 80 – 90 % reduction in vertical acceleration. Aluminum foam-based sacrificial claddings show high energy absorption capability when tested on a rigid structure [11], [15], [23], [30]. Sun et al. [23] experimentally investigated the deformation and failure modes of aluminum foam-based sandwich panels under blast loading. The blast tests were conducted using different face sheet materials, namely aluminum alloy, steel, and carbon fiber-reinforced plastic (CFRP). The crushable cores involved uniform and graded foam. It was shown that sandwich panels with CFRP front face sheets performed better. Their research also indicated that the blast resistance of panels with a positive gradient of core density (i.e., a core density that decreases linearly along the blast direction) is superior to those with a negative gradient of core density. Besides, the performance increases mainly when the difference in core density is important. To take into account the geometry of the underside of a vehicle, Shen et al. [31] investigated experimentally curved aluminum foam-based sandwich panels under blast loading. Curvature had three effects on the blast response of sandwich panels: it lowered the effective impulse imparted to the bottom plate, added a new failure mechanism of wrinkling, and added a new deformation regime with coupled circumferential bending and longitudinal stretching.

Sandhu et al. [32] investigated the mitigation of blast-induced acceleration by using add-on layers of polyurethane-based and rubber-based foams on a rigidly fixed composite plate under different blast loading intensities. The blast load was changed by varying the amount of C4 from 0.15 kg to 0.55 kg. The induced vibration in the composite plate produced by blast wave impingement was quantified in terms of acceleration using a piezoelectric

accelerometer. Maximum acceleration mitigation of about 50 % and 80 % was observed for 200 mm of polyurethane-based foam and rubber-based foam, respectively. Most of the research on using sacrificial cladding to increase the blast-resistance of an armored vehicle mainly focuses on the attenuation of acceleration. However, the deformation of the bottom plate of the vehicle is equally important to attenuate. Deformation of the bottom plate will apply significant axial load to the passenger resulting in lower limb, pelvic and spinal fractures [33]. Additionally, research on the effectiveness of mineral foam as a crushable material is rather limited. Jonet et al. [28] investigated the feasibility of using brittle mineral foam instead of polymeric or metallic foams as a crushable core of a sacrificial cladding for the protection of structures against an explosion event. The brittle mineral foam is from the same family of materials as autoclaved cellular concrete. In their research, Liu et al. [34] found an autoclaved cellular concrete to be strain rate sensitive. Two typical failure modes of autoclaved cellular concrete specimen were observed. When the strain rate was less than 10^{-2} s^{-1}, the specimen broke into several large pieces. This is due to the fact that with low-rate deformation, two or three major cracks can fully develop through the entire specimen. When the strain rate exceeded 10^{-2} s^{-1}, the specimen was broken into numerous small pieces and even crushed into powders. This is because micro cracks cannot develop into large cracks during the fast deformation process under high-speed impact. Many smaller cracks were formed to dissipate the impact energy, resulting in a large number of fragments.

This paper aims to evaluate the blast absorption capacity of brittle mineral foam when used as the crushable core of a sacrificial cladding for an armored vehicle. The absorption capacity of the foam core is investigated in terms of both the reduction of the deformation and out-of-plane displacement acceleration of a fixed aluminum plate representing the underside of a vehicle, i.e., the structure to protect. Previous research conducted by Olson et al. [35] reported failure modes for blast-loaded metallic square plates. By monotonically increasing the impulse, three different failure modes were identified, i.e., large inelastic deformation, tensile tearing of the boundary edges, and transverse boundary shear. Sprangers et al. [36] observed large inelastic deformation for a 3 mm thick aluminum plate (EN AW 1050A – H24) subjected to blast loading. The blast load was obtained by detonating 40 g of C4 set at 250 mm from the center of the tested material. In this work, large inelastic deformation of the aluminum plate is also aimed at. Therefore, the explosive charge mass and the stand-off distance will be chosen accordingly. Initially, the dynamic response of a non-protected aluminum plate subjected to blast loading is examined. Subsequently, the plate is studied with the addition of a foam layer with thicknesses of 60 mm and 120 mm. The explosive charge and the distance between the aluminum plate and the charge are fixed, as is the distance between

a vehicle's underside and a potential threat. Therefore, the thicker the foam layer, the smaller the distance between the charge and the sacrificial cladding, and the higher the loading will be.

The present paper is divided into four parts. First, the material properties of the main structure and of the crushable cores are presented. Second, a detailed description of the experimental set-up and the loading is given. Third, the effectiveness of the mineral foam as a crushable core is demonstrated. Finally, conclusions and perspectives on future work are given.

2. Experimental blast campaign

2.1. Materials

2.1.1. Aluminum plate

Plates serving as the main structure and as front skin were made from low-strength, strain-hardened, cold-rolled aluminum sheets of the alloy EN AW 1050A – H24. This is 99.5% pure aluminum subjected to annealing before being work hardened by rolling. Louar et al. [37] investigated the mechanical properties of EN AW 1050A – H24 by performing uniaxial tensile tests on 2 mm thick specimens. The study compared the material behavior in the longitudinal (0°) and transversal (90°) directions with respect to the rolling direction of the plate. It was concluded that the material is nearly isotropic with only a small variation both in yield stress and failure strain. **Table 1** includes the static mechanical properties of this aluminum alloy.

Table 1 Mechanical properties of aluminum alloy EN AW – 1050 H24 [37]

Density (kg/m^3)	**Young's Modulus (GPa)**	**Yield strength (MPa)**	**Tensile strength (MPa)**
2710	69	75	115

2.1.2. Mineral foam

The foam used in this work is a closed-cell micro-structure foam based on brittle mineral materials. It has a density of 110 kg/m^3 and a porosity of 95%. The foam is a mixture of calcium silicate hydrate (70 – 80 % weight concentration w/w), quartz (< 2 % w/w), calcite (15 – 20 % w/w), and gypsum (3 – 8 % w/w) that is stabilized in an autoclave under a pressure of 12 bar and a temperature of about 190 °C. Based on three uniaxial quasi-static

compression tests using a displacement velocity of 1 mm/min, the following properties are found: Young's modulus of 30 ± 2 MPa, a plateau stress of 237 ± 11 kPa, and a densification strain of 72 ± 1 % [29].

2.2. Experimental set-up

To study the absorption capacity of the brittle mineral foam, the set-up in Figure 1 (a) is used. The experimental set-up consists of a steel-rigid frame (1000 mm × 1000 mm × 15 mm) and a square cavity of 300 mm x 300 mm in the center. The square plate specimen (Figure 1 (b)) with a total surface of 400 mm × 400 mm and a thickness of 2 mm is clamped into the steel frame. This clamping is ensured by using bolted connections and a clamping frame (Figure 2 (a)) in an attempt to achieve fixed boundary conditions.

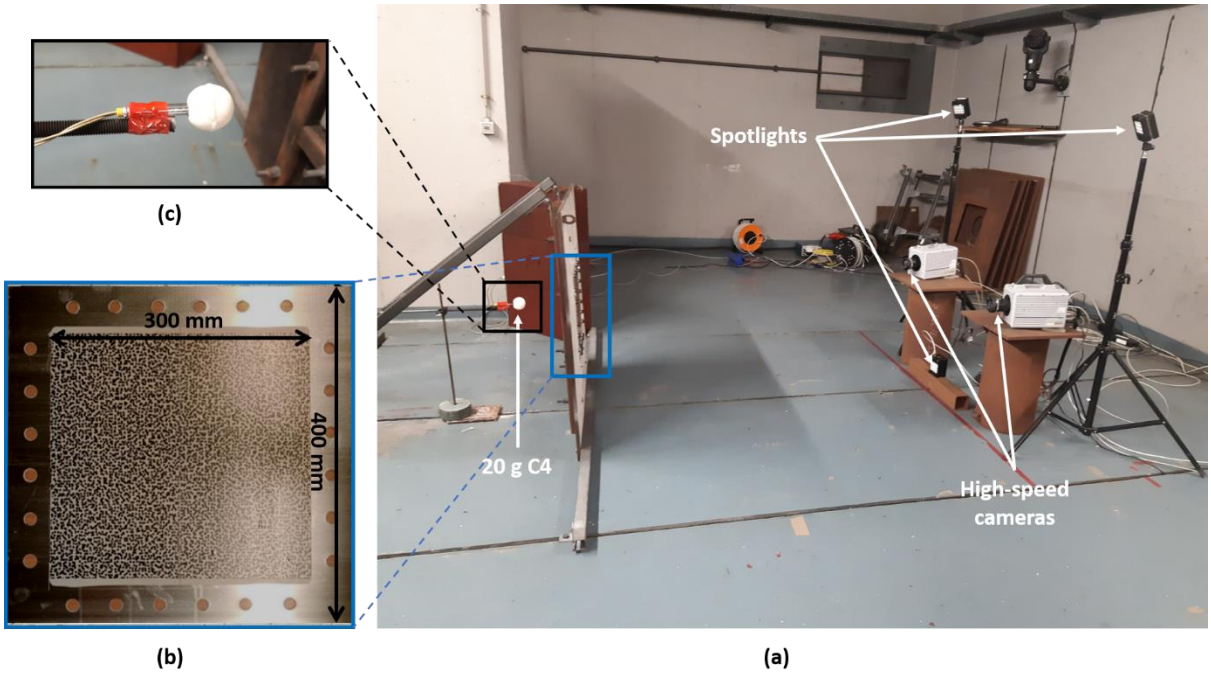

Figure 1. (a) Global view of the experimental set-up with the steel frame, two high-speed cameras in a stereo configuration, and three spotlights; (b) Tested aluminum (EN AW – 1050 A H24) plate painted with a speckle pattern to measure the out-of-plane displacement and in-plane strain field; and (c) spherical explosive and electronic detonator

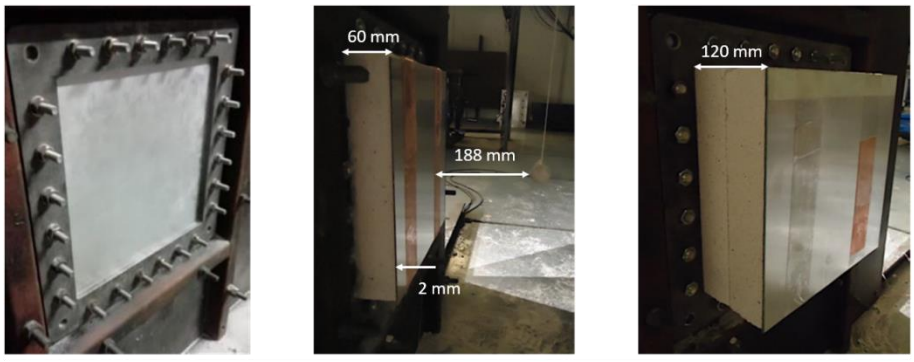

Figure 2. Tested aluminum backplates (a) without foam; (b) with 60 mm thick mineral foam and 2 mm aluminum front skin; and (c) with 120 mm thick mineral foam and 2 mm aluminum front skin

Two Photron Fastcam high-speed cameras are placed in a stereoscopic configuration, at an equal distance of 1100 mm from the center of the aluminum plate. The recording of the images at a frame rate of 20000 frames per second is triggered by the intentional rupture of an electric cable situated at the center of the explosive charge. This discontinuity in the electric current will initiate the recording of the dynamic behavior of the tested plate. The shutter time is 1/59000 second. Since important out-of-plane displacements (OPDs) are expected, an increased depth of view is sought by reducing the aperture of both lenses. To counterbalance the limited aperture of the shutter, three led lights are used to illuminate the area of interest. Aiming to fully capture the response of the plate at a surface of 400 × 400 mm², the resolution of the images is set to 512 × 512 pixels. This yields a pixel size of 0.78 mm/pixel. For the digital image correlation (DIC) post-process, a subset size of 21 × 21 pixels is used with a subset spacing of 3 pixels and a strain filter of 15.

The absorption capacity of the brittle mineral foam is assessed by comparing the dynamic response of the non-protected clamped aluminum plate to that of the plate retrofitted with different layers of mineral foam. The blast load is obtained by detonating 20 g of C4 placed 250 mm from the center of the tested material. The mass of the explosive charge and the stand-off distance are chosen to guarantee large inelastic deformation of the used aluminum plate. An electronic detonator (1 g of PETN) is used to initiate the detonation. A detail view of the explosive charge, the detonator, and its position is shown in Figure 1 (c).

The foam samples are characterized by a cross-section of 300 mm × 300 mm (cut from panels with a thickness of 60 mm) and two thicknesses, i.e., 60 and 120 mm, as shown in Figure 2 (b) and Figure 2 (c), respectively. Thus, to make 120 mm thick samples, two 60 mm thick foam samples are stacked. To fix the mineral foam, a double-sided self-adhesive tape is used. This adhesive tape is applied to both the aluminum backplate and the front skin.

By affixing the mineral foam with this tape on both sides, it is ensured a reliable attachment between the foam and the aluminum components without increasing the strength of the whole structure. The resultant stand-off distances (between the explosive charge and the front skin) are 188 mm and 128 mm respectively, taking into account the thickness of 2 mm of the aluminum front skin.

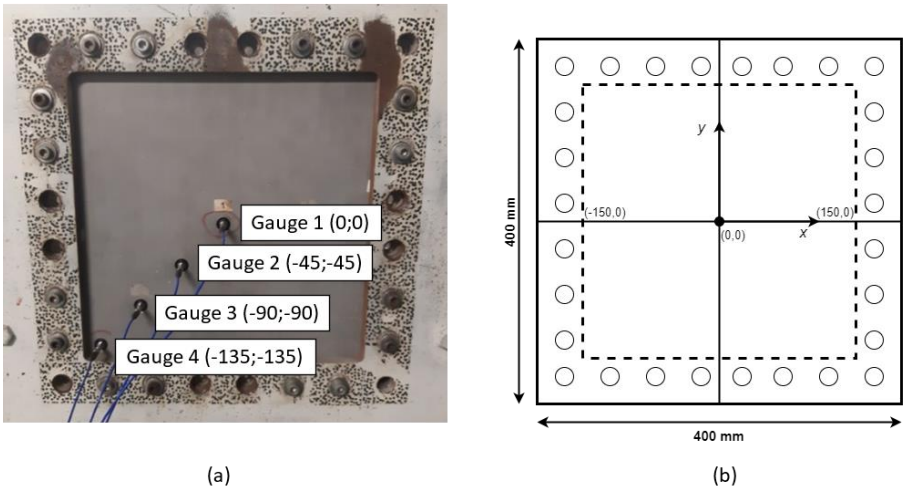

Figure 3. (a) Thick aluminum plate equipped with four high-pressure transducers; and (b) Schematic of the geometry of aluminum plate specimen

Prior to testing the 2 mm thick aluminum plates under blast loading, tests are carried out on an aluminum plate with a thickness of 15 mm. The main goal of these experiments is to examine the pressure distribution on a rigid plate and use those measurements to investigate the pressure distribution on the front skin as a function of the stand-off distance. The reflected pressure–time signals are measured for a charge of 20 g of C4 using piezoelectric pressure sensors integrated into the plate. The charge is set at 250 mm, 188 mm, and 128 mm, corresponding to the configuration without foam, with a 60 mm and a 120 mm thick foam layer, respectively. Figure 3 (a) shows the location of the four high-pressure transducers (PCB QUARTZ ICP 102B04). They are positioned at coordinates (0,0), (-45, -45), (-90, -90), and (-135, -135) with respect to the axes indicated in Figure 3 (b). In order to evaluate the reproducibility, each test per charge distance is performed three times.

3. Discussion of the results

3.1. Free-air blast loading

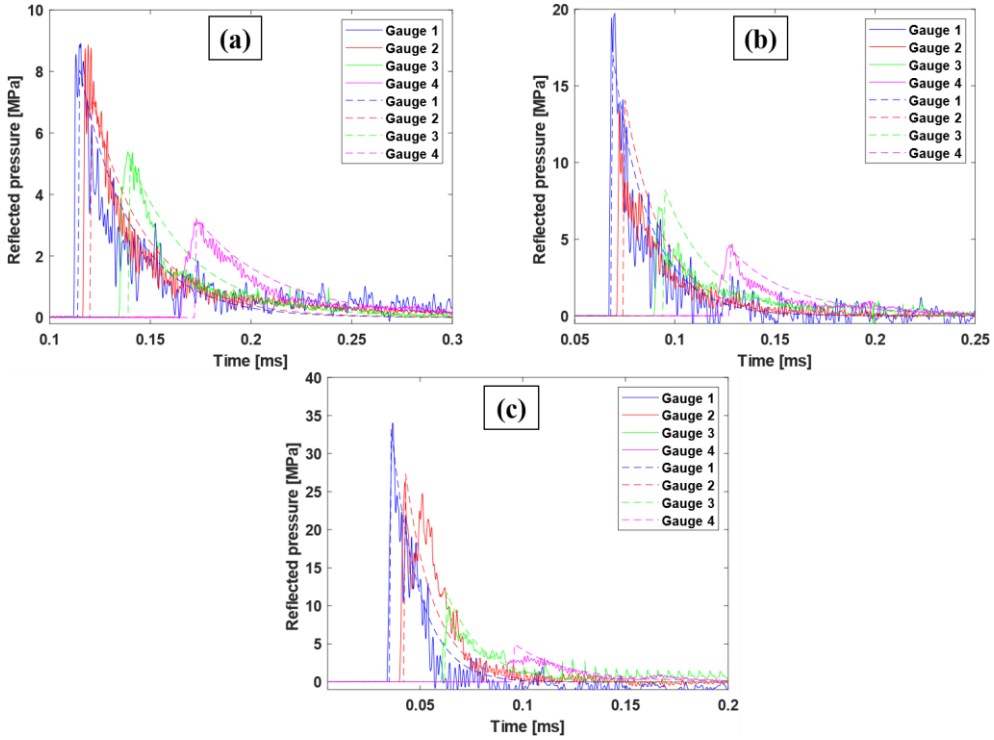

Figure 4. Pressure-time histories for 20 g of C4 set at (a) 250 mm; (b) 188 mm; and (c) 128 mm. The full lines are the measured pressures, while the dashed lines are the predicted ones

Figure 4 shows the pressure-time history recorded by the different pressure sensors under the three loading conditions. For the same loading conditions, reflected pressures are predicted using Kingery and Bulmash's empirical model [38]. This empirical model is widely used as an engineering tool for predicting blast waves and provides accurate estimates of maximum reflected over-pressures. The empirical data for air burst are valid for the range of scaled distance Z between 0.147 $m.kg^{-1/3}$ and 40 $m.kg^{-1/3}$ [39], where Z is the ratio between the distance from the charge center to the target and the TNT equivalent mass of the charge. For the studied configurations, Z is equal to 0.438 $m.kg^{-1/3}$ for the smallest stand-off distance and 0.855 $m.kg^{-1/3}$ for the largest one.

The results reveal that the air burst model's accuracy in terms of sphericity and amplitude of reflected pressure is adequate, which supports the premise that the blast wave has a spherical shape and expands in radial directions. The results also demonstrate that the empirical model slightly underestimates the shock wave's velocity, as shown in Figure 4. In Figure 4, it is intentionally chosen to represent only one signal to prevent graph overcrowding and maintain visual clarity. Including multiple signals for each charge distance would make the graph too congested

and difficult to interpret. Compiled peak pressures and impulses, along with their respective standard deviation, are shown in Figure 5. As the stand-off distance decreases, the blast load becomes more intense and localized.

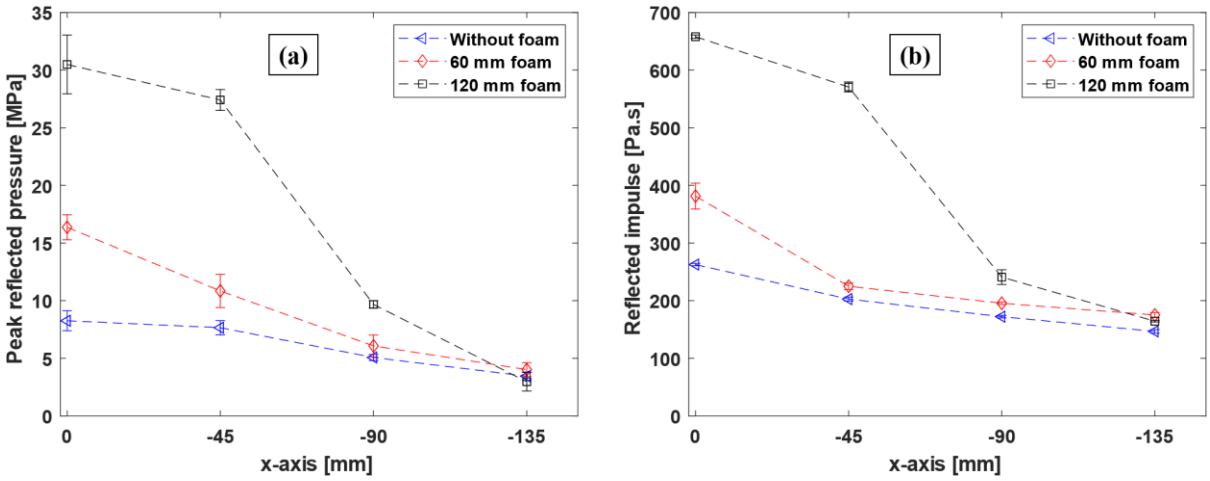

Figure 5. Compilation for various charge locations of the (a) peak reflected pressure, and (b) reflected impulse with an indication of the variability obtained at each gauge

3.2. Response of the backplate without foam

Figure 6 shows the cross-sectional OPD, velocity, and acceleration profiles of the backplate. 3D high speed DIC is used to gather the experimental data. After detonation, the pressure wave travels through the air to the backplate, resulting in a transient distribution load (see Figure 4(a)). Without the protective foam, the backplate is uniformly accelerated at 0.2 ms due to momentum transfer. The plate's material points are all forced to move out of the plane at given velocities. Areas close to the boundaries are constrained. Therefore, they have a very limited initial velocity (note that the profiles are shown from -100 mm to 100 mm, while the boundaries are located at -150 mm and 150 mm). As a result, the plate begins to deform into a rectangular shape. Additionally, due to the constraints at the boundaries, the plate experiences a sudden deceleration at 0.35 ms that propagated from the boundaries to the plate's center. The plate deforms further due to the inertial forces on its distributed mass, with the rectangular shape of deformation evolving towards a sinusoidal shape with a maximum OPD of 22 mm at approximately 0.8 ms. When the reaction forces overcome the inertial forces of the plate's mass, the material points of the plate are given negative velocities from the edges to the center, reaching a minimum of -25 m/s at 0.95 ms. From Figure 6(b), it is clear that the deformation history consists of mainly three major parts. At the beginning of the event, from 0 ms to 0.9 ms, the deformation is highly plastic and attains a peak value. This initial peak is followed by an elastic rebound, i.e., the recovery part [40], and elastic vibrations. Finally, a certain level of plastic deformation is observed. During the inbound and rebound phases, the largest acceleration is around 650 m/s² and 800 m/s², respectively.

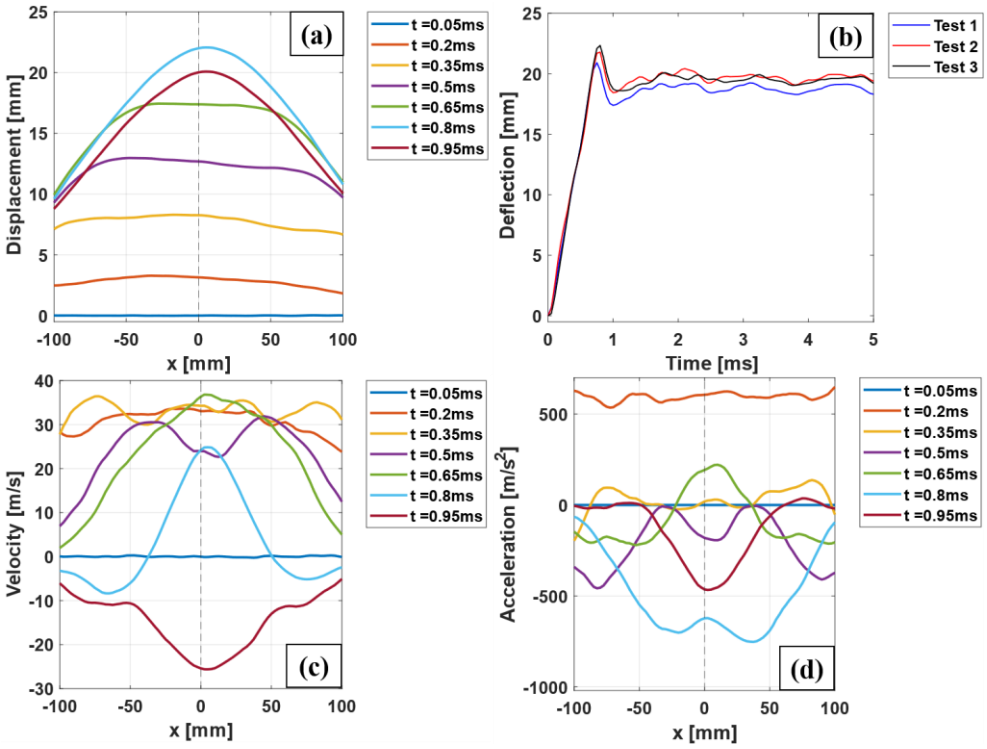

Figure 6. Response of the unprotected backplate (a) out-of-plane displacement profiles; (b) mid-span deflection; (c) velocity profiles; and (d) acceleration profiles

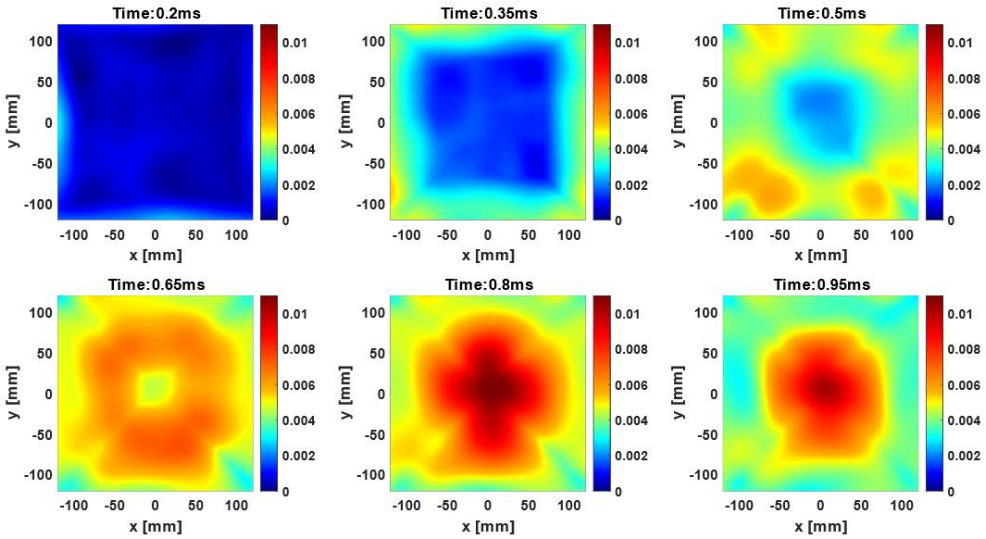

Figure 7. Major principal strain field ε_1 $(-)$ of the backplate without foam from 20 g of C4 at different time steps

Figure 7 depicts the evolution of the major principal strain ε_1. The largest strains occur close to the boundaries until time 0.45 ms. As previously stated, the blast impulse drives the entire plate to move out of the plane. Areas near the clamping boundaries are restrained. Higher strains occur in these areas. Furthermore, when inertia forces take over, strains occur in the center of the plate, reaching maximum values of 1.2 %, corresponding to large inelastic deformation, as reported by Olson et al. [35].

3.3. Influence of the foam on the backplate response

In this section the dynamic structural response of the backplate, retrofitted with the foam is investigated. The OPD, velocity, and acceleration are calculated for the two foam configurations, as shown in Figures 8 and 9. When the foam is added, the profiles of OPD, velocity, and acceleration are similar to those without foam protection. There is, however, a minor delay caused by the additional time required for the blast wave to pass through the foam core. A reduction in both the maximum deflection and velocity of the backplate can be observed. With 60 mm thick foam protection, the deflection at the center of the plate is roughly 12 mm, a reduction of 46%, while the reflected pressure and impulse rise by 123% and 45%, respectively.

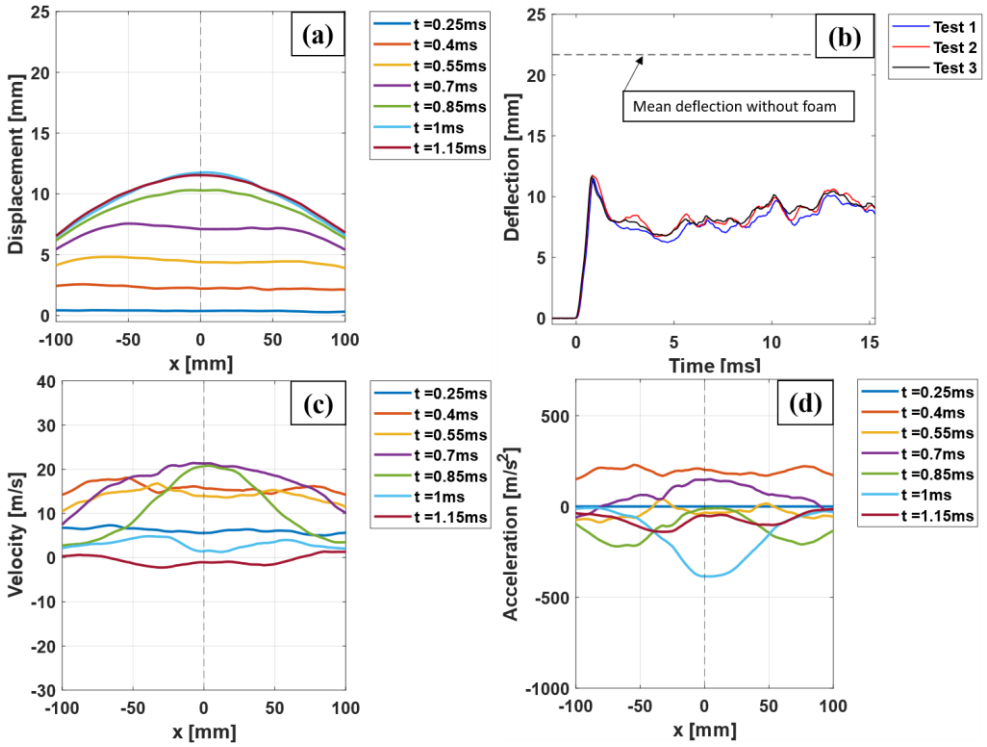

Figure 8. Backplate profile with 60 mm thick foam along x-axis of the (a) out-of-plane displacement profiles; (b) mid-span deflection; (c) velocity profiles; and (d) acceleration profiles

When the thickness of the foam is doubled, the deflection decreases to around 10 mm, a reduction of 54%, while the reflected pressure and impulse increase by 327% and 150%, respectively. It is also worth noting that the more foam is added, the more significant the recovery part is before oscillating till a permanent plastic displacement. Despite the increased loading due to adding foam and therefore reducing the stand-off distance, the transmitted load to the structure decreases.

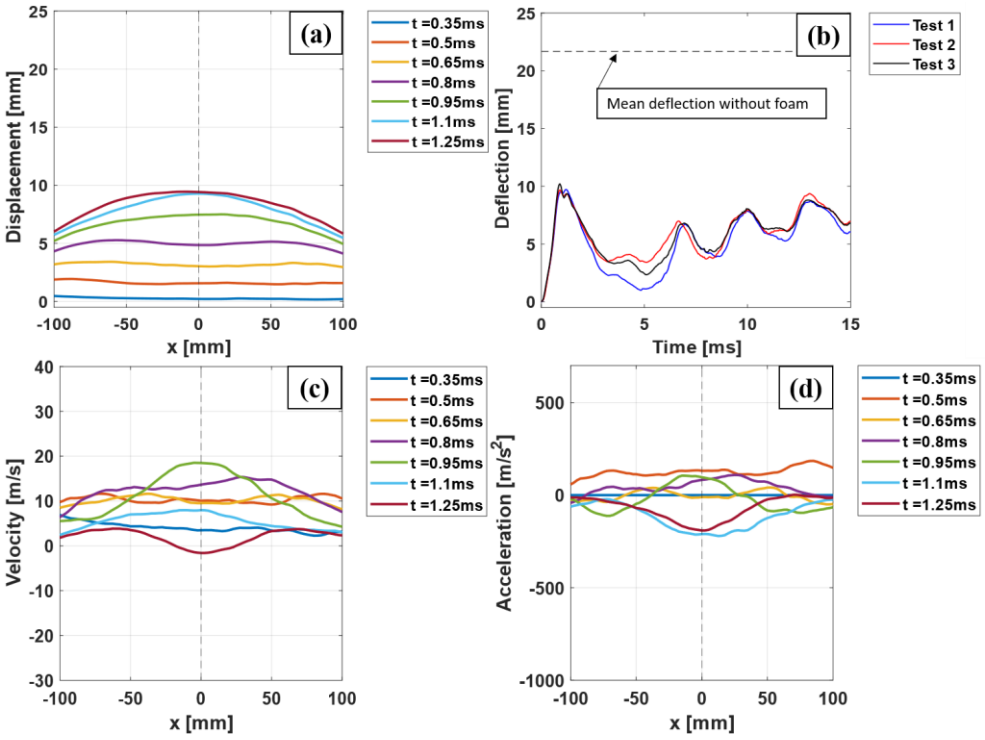

Figure 9. Backplate profile with 120 mm thick foam along x-axis of the (a) out-of-plane displacement profiles; (b) mid-span deflection; (c) velocity profiles; and (d) acceleration profiles

Unlike the case without foam protection, the region of the backplate that experiences relatively high velocity and acceleration seems to be reduced towards the center of the plate when the protective foam layer is added. In Figure 6(c), almost the entire area between -100 mm and 100 mm experiences a displacement velocity of more than 30 m/s. When a 60 mm thick foam layer is added, only the plate's area from -75 mm to 75 mm experience a velocity of more than 15 m/s as shown in Figure 8(c), half of the value for the plate without foam. Adding a 120 mm thick foam layer reduces the region that experiences more than 15 m/s to a range from -30 mm to 30 mm as shown in Figure 9(c). This can be explained by the fact that the loading becomes more localized when increasing the foam thickness.

Table 2 summarizes the values of maximum OPD, velocity, and accelerations of the backplate for the different foam thicknesses. The blast load rises with the foam thickness increasing, as discussed in Section 3.1. From **Table 2**, it can be concluded that adding brittle calcium-silicate-based mineral foam reduces maximum OPDs, velocity, and accelerations of the backplate at least by a factor of two.

Table 2 Summary of pressure, impulse, OPD, velocity, and acceleration results

Foam thickness (mm)	p_R **(MPa)**	i_R **(Pa.s)**	**Maximum OPD (mm)**	**Max velocity (m/s)**	**Max acceleration (m/s^2)**	
					The inbound phase	**The rebound phase**
0	7.3	235.1	21.7 ± 0.7	40.3 ± 2.3	690 ± 14	792 ± 18
60	16.3	388.9	11.6 ± 0.1	21.2 ± 0.7	276 ± 5	441 ± 8
120	32	615.6	9.9 ± 0.2	16.7 ± 2.3	250 ± 14	289 ± 20

Regarding the major principal strain values reached in the backplate with the protective foam, they are greatly attenuated, as illustrated in Figures 10 and 11. From Figure 10, it can be seen that maximum values are still attained in the central region of the plate. Adding a 60 mm thick foam layer reduces the maximal major principal strain from 1.2 % to 0.43 %, i.e., a reduction of 64%. When 120 mm thick foam layer is added, the maximum major principal strain reduces to 0.33%, i.e., a reduction of 73%.

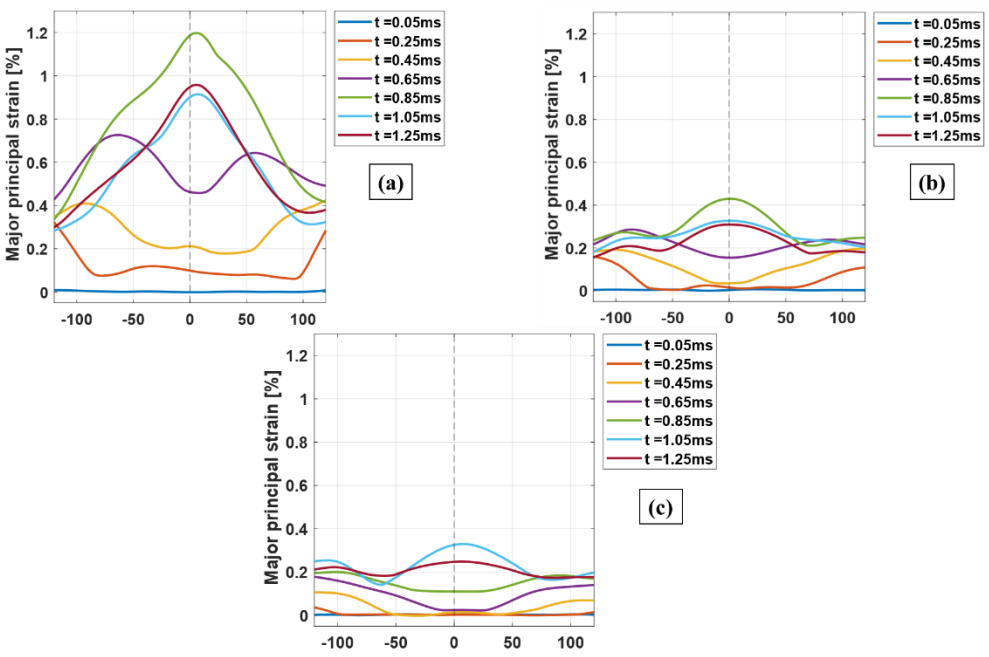

Figure 10. Major principal strain profile ε_1 (%) of the backplate from 20 g of C4 at different time steps: (a) without foam; (b) with 60 mm thick foam and (c) with 120 mm thick foam

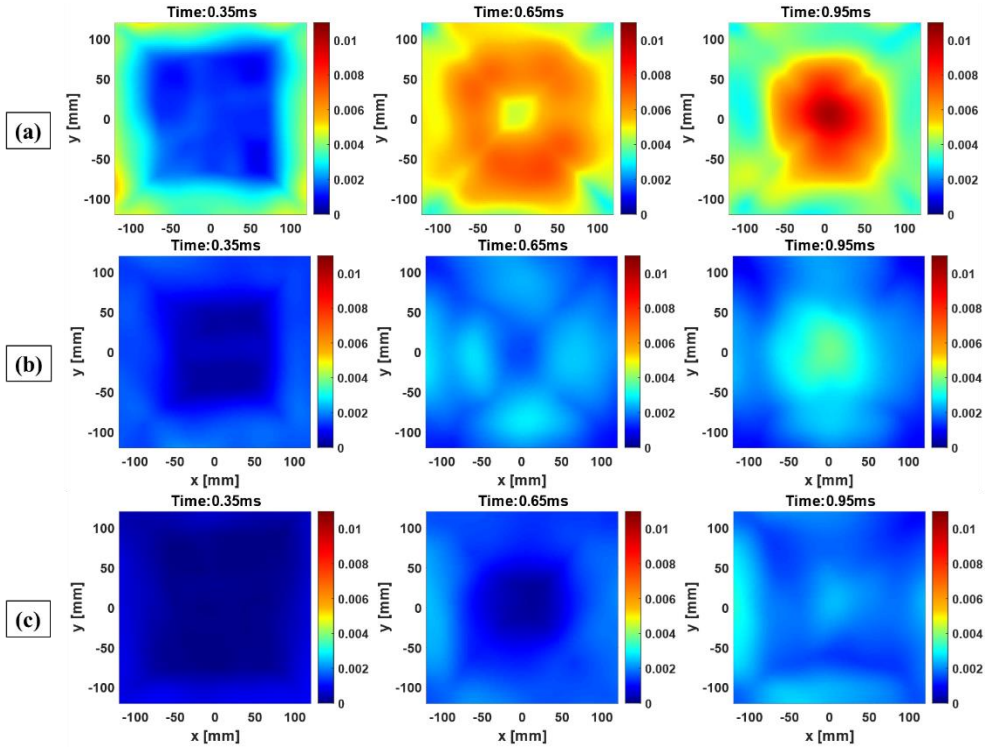

Figure 11. Comparison between major principal strain ε_1 $(-)$ of the backplate from 20 g of C4 at different time steps: (a) without foam; (b) with 60 mm thick foam and (c) with 120 mm thick foam

3.4. Foam mechanism of failure

Images of tested foams are shown in Figure 12. Two typical failure modes of the calcium-silicate-based foam subjected to blast loading can be observed. Depending on the loading intensity, the mineral foam experiences relatively low and high initial crushing velocity since the mass of the front skin is kept constant. At relatively low initial crushing velocity, i.e., with a 60 mm thick foam layer, there are a lot of large lumps of uncrushed material left. In fact, few major cracks developed through the whole specimen, as shown in Figure 12(a). When 120 mm thick foam is used, the lumps are even larger (Figure 12(b)) for the foam layer adjacent to the backplate, while the first-loaded layer has almost completely disintegrated.

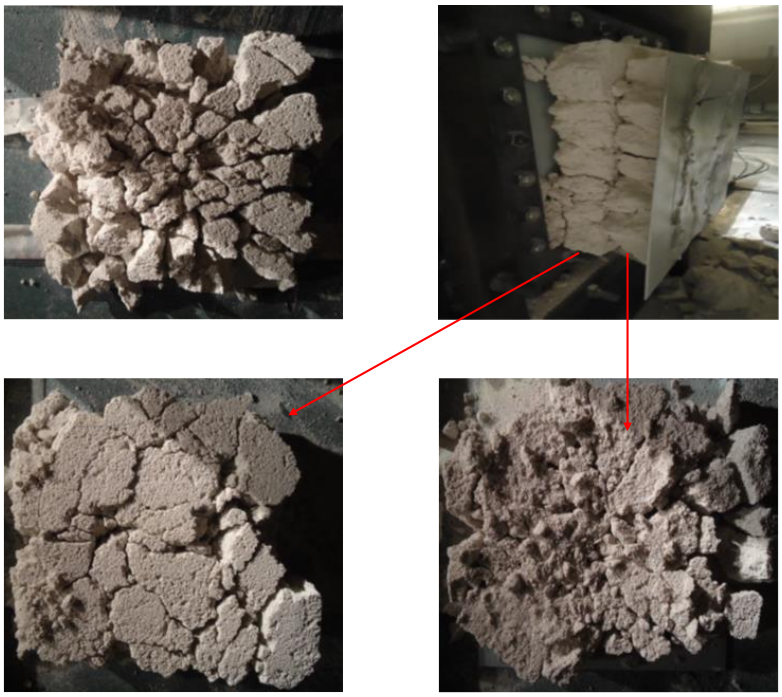

Figure 12. Mechanism of failure of (a) 60 mm thick foam and (b) 120 mm thick foam

When the foam experiences higher initial crushing velocity, micro-cracks cannot develop into large cracks during the fast deformation process. The sample disintegrates as a result of the formation of lots of smaller cracks. On the other hand, the foam layer adjacent to the backplate experiences lower compression rates compared to the configuration with 60 mm thick foam, resulting in larger lumps. Similar failure modes were observed on autoclaved aerated concrete in [34]. Investigation of what remains of the foam core reveals a non-optimal use of the foam core material. It shows that an optimal use of the mineral foam could have dissipated more energy through core disintegration.

4. Conclusions

In this paper, the absorption capacity of brittle calcium-silicate based-mineral foam is investigated by comparing the blast response of a clamped aluminum plate, representing the structure, with and without mineral foam. A series of blast tests is conducted by detonating 20 g of C4 set at a distance of 250 mm from the center of the backplate. Two foam thicknesses were considered: 60 mm and 120 mm. Since the distance between the structure and the explosive is kept constant, the analysis of the pressure distribution on the front skin reveals that the blast load becomes more intense and localized when increasing the foam thickness. The DIC technique has been successfully used to monitor the dynamic response of the tested specimens. When applying this type of mineral foam as the crushable core for sacrificial cladding protection, it has been proven to yield promising results.

The results reveal a reduction of OPD, velocity, and accelerations by at least a factor of two when the mineral foam layer, i.e., thickness of 60 mm and 120 mm, is added. The region of the backplate that experienced relatively high out-of-plane displacement velocity and acceleration is reduced to the central part of the backplate when the protective foam layer is added.

The maximum in-plane strains occur at the boundaries of the backplate at the beginning of the loading process due to the clamping of the backplate. Ah the end of the process they occur in the central area of the backplate. At this moment, the shock wave has vanished and, the further deformation of the backplate is only driven by the imparted momentum. There is a reduction of the strains from 1.2 % for the unprotected plate to 0.43 % and 0.33 % when the backplate is protected with 60 mm and 120 mm thick foams, respectively.

Post-mortem analysis of the foams reveals that mitigation of the blast load is obtained through the growth of cracks in the specimen. The crack propagation is found to be crushing velocity sensitive. Large lumps of uncrushed material are left. By optimizing loading conditions and exploring compartmentalized solutions, the foam could dissipate more energy, thereby improving blast mitigation of the sacrificial cladding.

Acknowledgements

The authors are grateful to the staff of the Laboratory of Propellants, Explosives and Blast Engineering (PEBE) department of the Royal Military Academy (RMA) in Brussels for their support and assistance in performing the different steps of the experimental work.

Funding sources

This research did not receive any specific grant from funding agencies in the public, commercial, or not-for-profit sectors.

References

[1] E. Krzystała, A. Mężyk, and S. Kciuk, “Minimisation of the explosion shock wave load onto the occupants inside the vehicle during trinitrotoluene charge blast,” *Int J Inj Contr Saf Promot*, vol. 23, no. 2, pp. 170–178, Apr. 2016, doi: 10.1080/17457300.2014.966118.

[2] A. N. Pratomo, S. P. Santosa, L. Gunawan, and I. S. Putra, “Countermeasures design and analysis for occupant survivability of an armored vehicle subjected to blast load,” *Journal of Mechanical Science and Technology*, vol. 34, no. 5, pp. 1893–1899, May 2020, doi: 10.1007/s12206-020-0411-1.

[3] “Test Methodology for Protection of Vehicle Occupants against Anti-Vehicular Landmine Effects,” Apr. 2007. [Online]. Available: www.rta.nato.int

[4] T. Schunck, D. Eckenfels, and L. Sinniger, “Blast disruption using 3D grids/perforated plates for vehicle protection,” *Defence Technology*, Oct. 2022, doi: 10.1016/j.dt.2022.10.005.

[5] H. bin Xu and L. K. Chen, “Mitigation effects on the reflected overpressure of blast shock with water surrounding an explosive in a confined space,” *Defence Technology*, vol. 17, no. 3, pp. 1071–1080, Jun. 2021, doi: 10.1016/j.dt.2020.06.026.

[6] T. Schunck, M. Bastide, D. Eckenfels, and J. F. Legendre, “Blast mitigation by water mist: the effect of the detonation configuration,” *Shock Waves*, vol. 30, no. 6, pp. 629–644, Sep. 2020, doi: 10.1007/s00193-020-00960-1.

[7] C. Breda, S. Kerampran, M. Sturtzer, M. Arrigoni, and J. F. LEGENDRE, *Analysis of planar and spherical shock-wave mitigation by wet aqueous foams*. 2018.

[8] X. Luo, A. J. Aref, and G. F. Dargush, “Optimal Design of Bundled Layered Elastic Stress Wave Attenuators,” *Journal of Computing in Civil Engineering*, vol. 26, no. 3, pp. 387–395, May 2012, doi: 10.1061/(asce)cp.1943-5487.0000143.

[9] Y. Li, Z. Lv, and Y. Wang, “Blast response of aluminum foam sandwich panel with double V-shaped face plate,” *Int J Impact Eng*, vol. 144, Oct. 2020, doi: 10.1016/j.ijimpeng.2020.103666.

[10] S. Berger, O. Sadot, and G. Ben-Dor, “Experimental investigation on the shock-wave load attenuation by geometrical means,” *Shock Waves*, vol. 20, no. 1, pp. 29–40, Feb. 2010, doi: 10.1007/s00193-009-0237-3.

[11] Z. Q. Ye and G. W. Ma, “Effects of Foam Claddings for Structure Protection against Blast Loads,” *Defence technology*, vol. 14, pp. 433–40, 2018, doi: 10.1061/ASCE0733-93992007133:141.

[12] M. Aleyaasin, J. J. Harrigan, and S. R. Reid, “Air-blast response of cellular material with a face plate: An analytical-numerical approach,” *Int J Mech Sci*, vol. 91, pp. 64–70, 2015, doi: 10.1016/j.ijmecsci.2014.03.027.

[13] G. W. Ma and Z. Q. Ye, “Analysis of foam claddings for blast alleviation,” *Int J Impact Eng*, vol. 34, no. 1, pp. 60–70, Jan. 2007, doi: 10.1016/j.ijimpeng.2005.10.005.

[14] H. Ousji, B. Belkassem, M. A. Louar, B. Reymen, L. Pyl, and J. Vantomme, “Experimental Study of the Effectiveness of Sacrificial Cladding Using Polymeric Foams as Crushable Core with a Simply Supported Steel Beam,” *Advances in Civil Engineering*, vol. 2016, 2016, doi: 10.1155/2016/8301517.

[15] G. S. Langdon, D. Karagiozova, M. D. Theobald, G. N. Nurick, G. Lu, and R. P. Merrett, "Fracture of aluminium foam core sacrificial cladding subjected to air-blast loading," *Int J Impact Eng*, vol. 37, no. 6, pp. 638–651, Jun. 2010, doi: 10.1016/j.ijimpeng.2009.07.006.

[16] V. Kostopoulos, G. D. Kalimeris, and E. Giannaros, "Blast protection of steel reinforced concrete structures using composite foam-core sacrificial cladding," *Compos Sci Technol*, 2022, doi: 10.1016/j.compscitech.2022.109330.

[17] H. B. Rebelo, D. Lecompte, C. Cismasiu, A. Jonet, B. Belkassem, and A. Maazoun, "Experimental and numerical investigation on 3D printed PLA sacrificial honeycomb cladding," *Int J Impact Eng*, vol. 131, pp. 162–173, Sep. 2019, doi: 10.1016/j.ijimpeng.2019.05.013.

[18] M. Abada, A. Ibrahim, and S. J. Jung, "Improving Blast Performance of Reinforced Concrete Panels Using Sacrificial Cladding with Hybrid-Multi Cell Tubes," *Modelling*, vol. 2, no. 1, pp. 149–165, Mar. 2021, doi: 10.3390/modelling2010008.

[19] J. Bonsmann and W. L. Fourney, "Mitigation of Accelerations Caused by Blast Loading Utilizing Polymeric-Coated Metallic Thin-Walled Cylinders," *Journal of Dynamic Behavior of Materials*, vol. 1, no. 3, pp. 259–274, Sep. 2015, doi: 10.1007/s40870-015-0023-5.

[20] J. Bonsmann and W. L. Fourney, "The Effect of Polyurea Mass Ratio on the Acceleration Mitigation Capabilities of Dynamically Loaded Structures," *Journal of Dynamic Behavior of Materials*, vol. 1, no. 1, pp. 28–42, Mar. 2015, doi: 10.1007/s40870-015-0007-5.

[21] G. Imbalzano, S. Linforth, T. D. Ngo, P. V. S. Lee, and P. Tran, "Blast resistance of auxetic and honeycomb sandwich panels: Comparisons and parametric designs," *Compos Struct*, vol. 183, no. 1, pp. 242–261, Jan. 2018, doi: 10.1016/j.compstruct.2017.03.018.

[22] F. Usta, H. S. Türkmen, and F. Scarpa, "Low-velocity impact resistance of composite sandwich panels with various types of auxetic and non-auxetic core structures," *Thin-Walled Structures*, vol. 163, Jun. 2021, doi: 10.1016/j.tws.2021.107738.

[23] G. Sun, E. Wang, J. Zhang, S. Li, Y. Zhang, and Q. Li, "Experimental study on the dynamic responses of foam sandwich panels with different facesheets and core gradients subjected to blast impulse," *Int J Impact Eng*, vol. 135, Jan. 2020, doi: 10.1016/j.ijimpeng.2019.103327.

[24] C. Wu and Y. Zhou, "Simplified Analysis of Foam Cladding Protected Reinforced Concrete Slabs against Blast Loadings," *International Journal of Protective Structures*, vol. 2, no. 3, pp. 351–365, 2011.

[25] K. A. Brekken, A. Reyes, T. Børvik, T. Berstad, and M. Langseth, "Sandwich panels with polymeric foam cores exposed to blast loading: An experimental and numerical investigation," *Applied Sciences (Switzerland)*, vol. 10, no. 24, pp. 1–36, Dec. 2020, doi: 10.3390/app10249061.

[26] S. Gabriel, C. J. Von Klemperer, S. C. K. Yuen, and G. S. Langdon, "Towards an understanding of the effect of adding a foam core on the blast performance of glass fibre reinforced epoxy laminate panels," *Materials*, vol. 14, no. 23, Dec. 2021, doi: 10.3390/ma14237118.

[27] S. Vavilala, P. Shirbhate, J. Mandal, and M. D. Goel, "Blast mitigation of RC column using polymeric foam," *Mater Today Proc*, vol. 26, pp. 1347–1351, 2019, doi: 10.1016/j.matpr.2020.02.273.

[28] A. Jonet, B. Belkassem, O. Atoui, L. Pyl, and D. Lecompte, “Blast Mitigation Using Brittle Foam Based Sacrificial Cladding: A Feasibility Study,” in *18th international symposium for the interaction of the effect of munitions with structures*, 2019.

[29] A. Aminou, B. Belkassem, O. Atoui, D. Lecompte, and L. Pyl, “Numerical Modeling of Brittle Mineral Foam in a Sacrificial Cladding Under Blast Loading,” in *Congrès Français de Mécanique*, 2022, pp. 4540–4550.

[30] Y. Sun and Q. M. Li, “Dynamic compressive behaviour of cellular materials: A review of phenomenon, mechanism and modelling,” *Int J Impact Eng*, vol. 112, pp. 74–115, Feb. 2018, doi: 10.1016/j.ijimpeng.2017.10.006.

[31] J. Shen, G. Lu, Z. Wang, and L. Zhao, “Experiments on curved sandwich panels under blast loading,” *Int J Impact Eng*, vol. 37, no. 9, pp. 960–970, Sep. 2010, doi: 10.1016/j.ijimpeng.2010.03.002.

[32] I. S. Sandhu, M. Thangadurai, P. S. Alegaonkar, and D. R. Saroha, “Mitigation of Blast Induced Acceleration using open cell natural rubber and Synthetic Foam,” *Def Sci J*, vol. 69, no. 1, pp. 53–57, Jan. 2019, doi: 10.14429/dsj.69.12586.

[33] A. Ramasamy, A. Hill, A. Hepper, A. Bull, and J. Clasper, “Blast Mines: Physics, Injury Mechanisms And Vehicle Protection,” *BMJ Mil Health*, Sep. 2015, [Online]. Available: http://jramc.bmj.com/

[34] C. Liu, J. Hou, Y. Hao, H. Hao, and X. Meng, “Effect of high strain rate and confinement on the compressive properties of autoclaved aerated concrete,” *Int J Impact Eng*, vol. 156, Oct. 2021, doi: 10.1016/j.ijimpeng.2021.103943.

[35] M. D. Olson, G. N. Nurick, and J. R. Fagnan, “DEFORMATION AND RUPTURE OF BLAST LOADED SQUARE PLATES-PREDICTIONS AND EXPERIMENTS,” *Int. J. hnpact Enqng*, vol. 13, no. 2, pp. 279–291, 1993.

[36] K. Spranghers, I. Vasilakos, D. Lecompte, H. Sol, and J. Vantomme, “Full-Field Deformation Measurements of Aluminum Plates Under Free Air Blast Loading,” *Exp Mech*, vol. 52, no. 9, pp. 1371–1384, Nov. 2012, doi: 10.1007/s11340-012-9593-5.

[37] M. A. Louar, “Estimation of the strain rate hardening model parameters of GFRE using blast loads and inverse modelling,” Royal Military Academy, Brussels, 2017.

[38] G. F. Kinney and Graham Kenneth J, *EXPLOSIVE SHOCKS IN AIR*, Second edition. New York: Springer science+Business Media New York, 1985. doi: 10.1007/978-3-642-86682-1.

[39] LSTC, *LS-DYNA KEYWORD USER’S MANUAL VOLUME I*, vol. I. 2017. [Online]. Available: www.lstc.com

[40] V. Aune, E. Fagerholt, K. O. Hauge, M. Langseth, and T. Børvik, “Experimental study on the response of thin aluminium and steel plates subjected to airblast loading,” *Int J Impact Eng*, vol. 90, pp. 106–121, Apr. 2016, doi: 10.1016/j.ijimpeng.2015.11.017.